ACS Catalysis

Research Article

pubs.acs.org/acscatalysis

Palladium Nanoparticles Encapsulated in Core−Shell Silica: A Structured Hydrogenation Catalyst with Enhanced Activity for Reduction of Oxyanion Water Pollutants

Yin Wang,[†,‡,∥] Jinyong Liu,[†,‡] Peng Wang,[§] Charles J. Werth,[†,⊥] and Timothy J. Strathmann*[,†]

[†]Department of Civil and Environmental Engineering, University of Illinois at Urbana−Champaign, Urbana, Illinois 61801, United States

[§]Water Desalination and Reuse Center, Biological and Environmental Sciences and Engineering Division, King Abdullah University of Science and Technology, Thuwal, Saudi Arabia

Supporting Information

ABSTRACT: Noble metal nanoparticles have been applied to mediate catalytic removal of toxic oxyanions and halogenated hydrocarbons in contaminated water using H_2 as a clean and sustainable reductant. However, activity loss by nanoparticle aggregation and difficulty of nanoparticle recovery are two major challenges to widespread technology adoption. Herein, we report the synthesis of a core−shell-structured catalyst with encapsulated Pd nanoparticles and its enhanced catalytic activity in reduction of bromate (BrO_3^-), a regulated carcinogenic oxyanion produced during drinking water disinfection process, using 1 atm H_2 at room temperature. The catalyst material consists of a nonporous silica core decorated with preformed octahedral Pd nanoparticles that were further encapsulated within an ordered mesoporous silica shell (i.e., SiO_2@Pd@mSiO_2). Well-defined mesopores (2.3 nm) provide a physical barrier to prevent Pd nanoparticle (~6 nm) movement, aggregation, and detachment from the support into water. Compared to freely suspended Pd nanoparticles and SiO_2@Pd, encapsulation in the mesoporous silica shell significantly enhanced Pd catalytic activity (by a factor of 10) under circumneutral pH conditions that are most relevant to water purification applications. Mechanistic investigation of material surface properties combined with Langmuir−Hinshelwood modeling of kinetic data suggest that mesoporous silica shell enhances activity by promoting BrO_3^- adsorption near the Pd active sites. The dual function of the mesoporous shell, enhancing Pd catalyst activity and preventing aggregation of active nanoparticles, suggests a promising general strategy of using metal nanoparticle catalysts for water purification and related aqueous-phase applications.

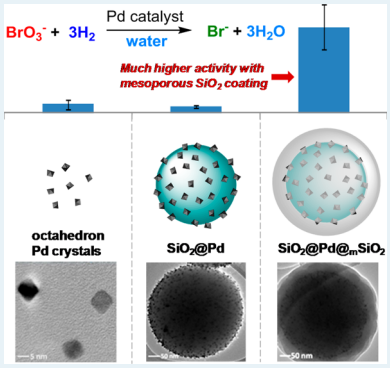

KEYWORDS: *palladium nanoparticle, mesoporous silica, core−shell, bromate, oxyanion, water purification*

1. INTRODUCTION

Palladium-based materials have wide application in the field of catalysis, because of their ability to facilitate a variety of reactions.[1−3] One emerging application is to use Pd-based catalysts in water purification and remediation processes for the reductive transformation of recalcitrants and emerging classes of aquatic contaminants, including halogenated organics, oxyanions, nitrosamines, and pharmaceutical and personal care products (PPCPs).[3−8] Recent developments in material science and technology have enabled the synthesis of Pd nanoparticles (NPs) with controllable shapes and sizes.[9−13] Pd NPs and Pd-based bimetallic NPs have been applied in catalyzing various aqueous reactions,[14,15] and have shown great potential as catalysts for water treatment and purification application, because of their unique properties, such as high surface area to volume ratio and quantum size effects.[16−18] Shuai et al. synthesized Pd NPs with various shapes and sizes and demonstrated their ability to catalytically reduce the oxyanion nitrite (NO_2^-), the disinfection byproduct N-nitrosodimethylamine (NDMA), and the halogenated pharmaceutical micropollutant diatrizoate,[18] all of which are highly resistant to treatment by conventional drinking water treatment technologies. However, a major challenge to the application of Pd NPs for water purification is the susceptibility of NPs that lack surface stabilizers to aggregate in water to form large bulk Pd precipitates, and particle aggregation negatively affects reactivity of the NPs.[19−21] In addition, Pd NPs are difficult to recover from water following application, because of their small size, and there are growing concerns about the release of such NPs into aquatic environments and associated ecological and public health risks.[22]

A variety of immobilization strategies are being investigated to overcome limitations and concerns associated with applying Pd NPs in aquatic systems. Core−shell support materials decorated with noble-metal NPs have drawn increased attention in heterogeneous catalysis, because of their unique

Received: July 8, 2014
Revised: September 1, 2014
Published: September 2, 2014

   dx.doi.org/10.1021/cs500971r | ACS Catal. 2014, 4, 3551−3559

Scheme 1. Preparation Procedure of the Core–Shell-Structured Silica Materials with Encapsulated Pd NPs

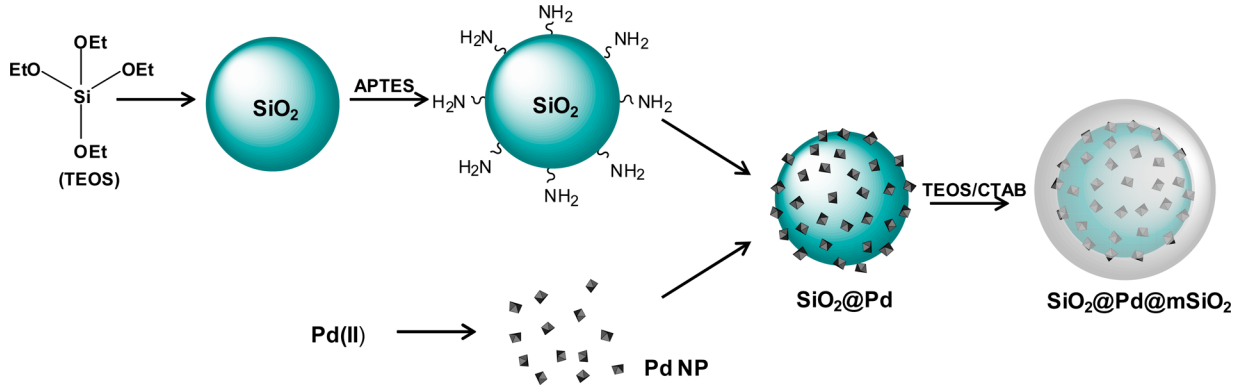

electronic features that affect catalytic activity, lack of aggregation in aqueous solution, and prevention of sintering at elevated temperatures (e.g., >350 °C).[23−25] Silica-based core–shell materials have received special attention, because of their high thermal stability and tolerance of acidic conditions.[26,27] Successful synthesis of several types of core–shell silica materials with immobilized noble-metal NPs has been reported.[28−31] Joo et al. developed a core–shell-structured nanocatalyst consisting of a single platinum (Pt) nanoparticle core coated with a mesoporous silica shell (i.e., Pt@mSiO_2).[23] They found that the presence of the mesoporous shell prevented the aggregation and Pt NP sintering at high temperature, thereby enhancing catalytic CO oxidation. Similarly, synthesis of a Pd-based core–shell-structured silica was reported with a single Pd NP core encapsulated in a mesoporous silica shell.[32] Although these materials have promise in gas-phase applications, their small size (i.e., <50 nm) prevents easy separation and recovery during water purification applications.

An alternative approach to increase the size of the material involves immobilization of a large number of metal NPs on a single silica core structure that is subsequently coated with a mesoporous shell to encapsulate the NPs (i.e., SiO_2@M@mSiO_2).[28,33] The mesoporous shell allows substrate access to the reactive metal NPs while enhancing thermal stability.[26] The mesoporous shell can be developed by a surfactant templating approach or by selective etching of a nonporous shell.[28,33] Recently, Wang et al. reported using the latter approach to synthesize core–shell silica with Pd NPs sandwiched between a nonporous silica core and a mesoporous silica shell.[34] NaOH was used to etch the nonporous silica shell, and the resulting material was characterized by a broad pore size distribution with a relatively large average pore size (i.e., >15 nm). In designing core–shell-structured supports for water purification applications, ideally the mesoporous shell will be highly porous, to allow the transport of reactants to encapsulated metal NPs, but individual pore sizes will be narrower than the size of metal NPs, to effectively prevent NP aggregation or release from the support material.

The primary objective of this contribution was to develop an advanced silica-based structure to enhance the suitability of Pd NPs in environmental catalysis application. We report the design, synthesis, and aqueous reactivity of a silica-based core–shell-structured material with encapsulation of shaped Pd NPs. A nonporous silica core was decorated with preformed octahedral Pd NPs that were further encapsulated within a surfactant-templated mesoporous silica shell developed through a NaOH-mediated hydrolysis approach (i.e., SiO_2@Pd@mSiO_2). The well-designed pore structure has a small pore size and narrow size distribution, and it makes the material highly suitable as a model catalyst for probing aqueous reactions. The catalyst was applied to remove bromate (BrO_3^-) as a model drinking water contaminant. Bromate is an EPA-regulated byproduct of drinking water disinfection processes, because of its nephrotoxicity and potential carcinogenicity.[35−37] To the best of our knowledge, this is the first report of the construction of SiO_2@Pd@mSiO_2 with a well-defined pore structure with Pd NPs constrained to the interface between the silica core and the mesoporous shell. More importantly, this work demonstrates, for the first time, that the presence of mesoporous silica shell enhances Pd catalyst reactivity with contaminants under aqueous conditions relevant to water purification applications.

2. RESULTS AND DISCUSSION

2.1. Synthesis and Characterization of SiO_2@Pd@mSiO_2. SiO_2@Pd@mSiO_2 microspheres were prepared in three steps (Scheme 1): (1) separate synthesis of shape-controlled Pd NPs and surface-functionalized nonporous silica microspheres, (2) immobilization of the preformed Pd NPs on the surface of the silica microspheres (SiO_2@Pd), and (3) growth of a surfactant-templated mesoporous silica shell on the SiO_2@Pd microspheres. A combination of techniques, described individually in detail in the Experimental Section, were used in the synthesis process, including sol–gel processing, interfacial deposition, and surfactant templating.

Pd NPs were synthesized by reducing Na_2PdCl_4 with citric acid, as reported previously.[13] Polyvinylpyrrolidone (PVP) was added to serve as a stabilizer to control the growth and prevent the aggregation of Pd NPs. As observed by transmission electron microscopy (TEM), the Pd NPs were mainly in an octahedral shape (>75%) with an edge length of ∼6 nm (see Figures 1A and 1B). The X-ray diffraction (XRD) pattern of the Pd NPs matched well with the face-centered cubic (fcc) Pd(0) crystal reference pattern (Figure 2). No crystalline phases other than Pd(0) were observed from XRD. The average Pd NP size was calculated as 6.2 nm from peak widths, according to the Debye–Scherrer equation, which is consistent with the observation from TEM.

Silica microspheres were synthesized using the Stöber method.[38] As shown in the scanning electron microscopy (SEM) image (Figure 3A), monodisperse silica microspheres with a diameter of ∼400 nm were obtained. Ammonia was added to provide basic conditions to facilitate tetraethylortho-

dx.doi.org/10.1021/cs500971r | ACS Catal. 2014, 4, 3551−3559

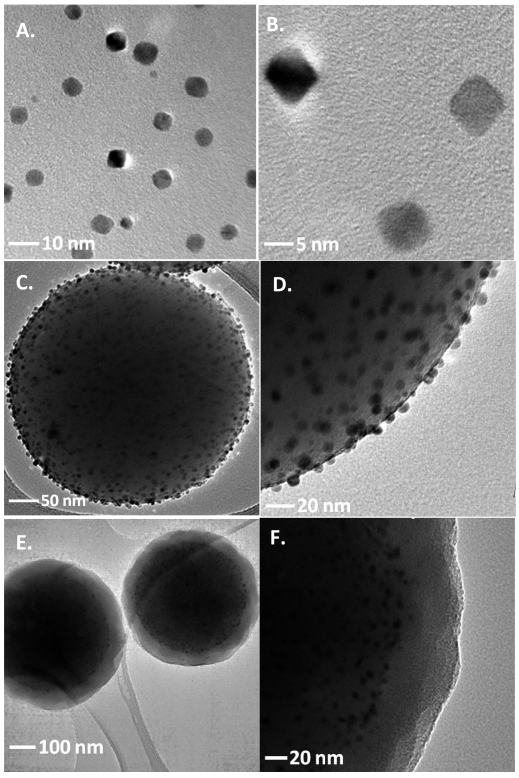

Figure 1. TEM images of (A, B) Pd NPs, (C, D) SiO_2@Pd microspheres, and (E, F) SiO_2@Pd@mSiO_2 microspheres.

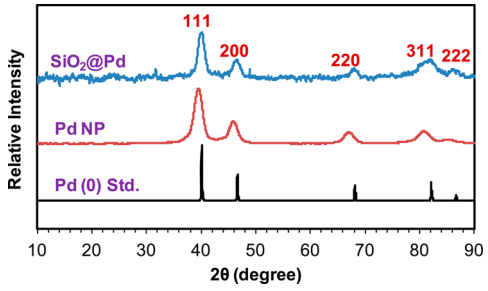

Figure 2. XRD pattern of the unimmobilized Pd NPs and Pd NPs deposited on the silica microspheres (SiO_2@Pd). The reference pattern for fcc Pd(0) crystal is included for comparison.

silicate (TEOS) hydrolysis and was also used to control the shape of the silica acquired. The synthesized silica microspheres had a spherical shape with smooth surface, as observed by SEM (Figure 3A). As previously reported, irregularly shaped silica particles were obtained if ammonia was not added.[38] To support immobilization of Pd NPs, the silica microsphere surfaces were further functionalized with amino groups using 3-aminopropyl triethoxysilane (APTES), because of the strong chemical interaction between the NPs and the $-NH_2$ group.[39−41] An oxygen-free environment was employed to prevent oxidation of the amino groups. As shown in Figure 3B, the size and the surface roughness of the silica microspheres were unchanged by $-NH_2$ functionalization.

SiO_2@Pd was obtained by mixing PVP-stabilized Pd NPs with $-NH_2$ functionalized silica microspheres in water. Pd NPs evenly covered the surfaces of silica microspheres in the resulting material (Figures 1C and 1D and 3C and 3D). The XRD pattern of SiO_2@Pd was similar to that of the free Pd NPs, and no Pd(II) crystalline phases were detected (Figure 2).

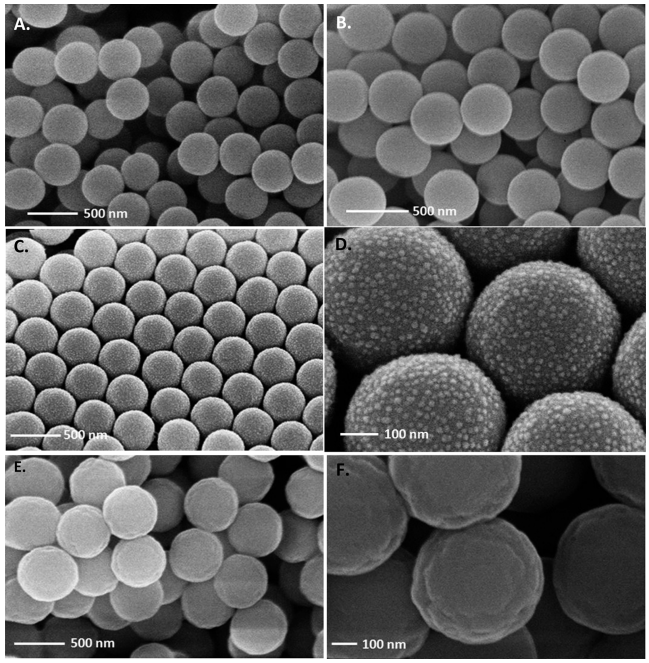

Figure 3. SEM images of (A) nonporous SiO_2 microspheres, (B) $-NH_2$ functionalized SiO_2 microspheres, (C, D) SiO_2@Pd microspheres, and (E, F) SiO_2@Pd@mSiO_2 microspheres.

Based on the Debye−Scherrer equation, the Pd particle size on SiO_2@Pd was calculated as 6.5 nm, which is in close agreement with measurements of the free Pd NPs. Results suggest that both the size and the crystal structure of the Pd NPs were preserved during immobilization on the silica core. For the SiO_2@Pd, the Pd NPs were strongly attached to the surface of the $-NH_2$-functionalized silica sphere. In addition to the interaction between Pd NP and $-NH_2$ group, PVP that is coated on the Pd NP surface might also facilitate the immobilization of Pd NPs by forming hydrogen bonds with $-NH_2$ groups on the silica surface or by modifying surface charge to enhance the electrostatic interactions.[42] Attempts to immobilize the Pd NPs on unfunctionalized and −SH-functionalized silica microspheres, which were previously reported to promote Au NP immobilization,[29,43] were unsuccessful.

The mass loading of Pd NPs immobilized on the silica surface can be tuned by adjusting the relative amounts of Pd NPs and $-NH_2$-functionalized silica microspheres (see Figure S1 in the Supporting Information (SI)). Almost all the Pd NPs in aqueous suspension were immobilized when their amount was <3 wt % of the $-NH_2$ functionalized silica microspheres, whereas further increases in the suspension concentration of Pd NPs did not yield higher Pd loadings on the silica microspheres. Elemental analysis confirmed that the maximum Pd concentration of SiO_2@Pd is 3.0 wt %. For such material, the surface was uniformly covered by a single layer of Pd NPs, as shown by SEM (Figure 3D). Note that the particle size as well as the solvent might affect the uniformity of metal nanoparticle deposition. Westcott and Halas reported that increasing ethanol-to-water ratios promote Au NP aggregation and cluster formation on the surface of silica.[29] Wang et al. reported nonuniform attachment and low surface coverage of Pd NPs deposited on silica microspheres in water, which is probably due to the larger Pd NP particle size (~20 nm) used in their study.[34] In the present work, the smaller size of the Pd NPs

dx.doi.org/10.1021/cs500971r | ACS Catal. 2014, 4, 3551−3559

combined with the use of water as the solvent yielded a more uniform distribution of Pd NPs on silica microsphere surfaces.

A surfactant templating method was used to grow mesoporous silica shells on the SiO_2@Pd microspheres. TEOS was hydrolyzed in the presence of SiO_2@Pd and hexadecyltrimethylammonium bromide (CTAB), a structure directing agent that promotes formation of a mesostructured CTAB/silica shell on the surface of the SiO_2@Pd microspheres.[44] The CTAB then was removed by extraction in a mixture of ethanol and concentrated HCl to obtain SiO_2@Pd@$mSiO_2$ microspheres.[45] The thickness of the mesoporous shell was ~60 nm and the Pd content of the SiO_2@Pd@$mSiO_2$ was determined to be 1.3 wt %. Instead of $NH_3{\cdot}H_2O$,[33] dilute NaOH (1.7 mM) was used as a base during the surfactant-templating procedure to catalyze TEOS hydrolysis and preserve the sphere shape of the mesoporous shell. With the use of NaOH, sandwich-structured SiO_2@Pd@$mSiO_2$ microspheres were obtained where Pd NPs were well-constrained at the interface between the silica core and shell materials (Figure 1E and 1F). In contrast, when using $NH_3{\cdot}H_2O$ as a base the majority of the Pd NPs were liberated from the surface of the inner silica core and distributed randomly throughout the emplaced mesoporous silica shell (see Figure S2 in the SI). The loss of Pd NPs from the core surface may be due to competing Pd interactions with $-NH_2$ groups on the silica surface and dissolved NH_3. Using NaOH to form the mesoporous shell also resulted in uniform silica spheres (see Figure 1E). Joo et al. also reported uniform core–shell-structured Pt@$mSiO_2$ spheres when adding diluted NaOH to catalyze surfactant-templated TEOS hydrolysis in the presence of free Pt NPs.[23] It is worth noting that previous studies report that higher NaOH concentrations (>0.5 M) may react directly with silica, etching the mesoporous silica structure and changing the pore size.[28,34]

The porous nature of the SiO_2@Pd@$mSiO_2$ microspheres was confirmed by measuring N_2 adsorption–desorption isotherms (Figure 4). The Brunauer–Emmett–Teller (BET) surface area was measured to be 480 m^2/g, and the total pore volume was estimated as 0.27 cm^3/g. Application of the Barrett–Joyner–Halenda (BJH) model confirmed that the surfactant templating approach yielded a highly uniform pore size distribution in the mesoporous shell with an average diameter of 2.3 nm (see Figure 4). The value is similar to that reported by Deng et al., who also used CTAB to form core–shell-structured Fe_3O_4@SiO_2–Au@SiO_2 microspheres with an average pore size of 2.2 nm.[33] Wang et al. synthesized SiO_2@Pd@$mSiO_2$ using a NaOH etching method without the addition of a surfactant template.[34] This resulted in a less-uniform pore size distribution and much larger average pore size (>15 nm) than that reported here. It is worth noting that the pore size obtained here is significantly smaller than the size of the preformed Pd NPs, thereby providing a physical barrier to prevent release of the NPs into solution. In addition, it is worth mentioning that the surfactant templating method may also result in a highly ordered pore orientation that is perpendicular to the core, since this preferred alignment of surfactant micelles and TEOS minimizes the overall interfacial energy of the system.[33,46,47]

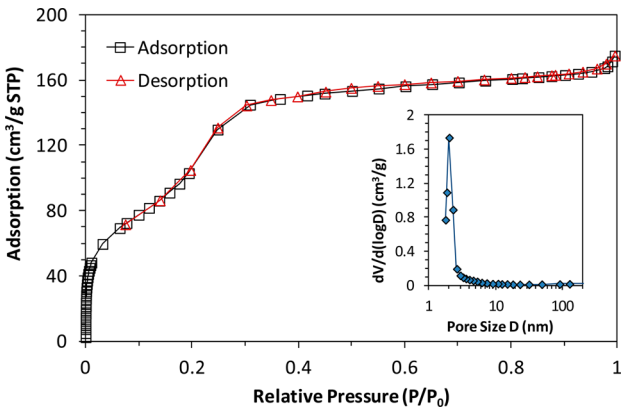

Figure 4. N_2 adsorption–desorption isotherms and pore size distribution (inset) of SiO_2@Pd@$mSiO_2$ microspheres prepared with an ~60-nm-thick mesoporous shell.

The thickness of the mesoporous shell can be controlled by adjusting the amounts of TEOS and CTAB. For example, increasing the TEOS concentration 2.4-fold during synthesis resulted in an increase of the mesoporous shell thickness from 60 nm to 120 nm (see Figures S3 and S4 in the SI). Interestingly, further increasing the TEOS concentration by another 50% resulted in a nonuniform coating of mesoporous silica shell, and SiO_2@Pd@$mSiO_2$ microspheres with multiple sizes were obtained (see Figure S4 in the SI).

2.2. Catalytic Reduction of Bromate. The activity of SiO_2@Pd@$mSiO_2$ in catalyzing the reduction of bromate (BrO_3^-) was measured and compared with that of free Pd NPs and SiO_2@Pd in H_2-saturated water at pH 7 and ambient temperature (20 ± 1 °C). The overall reaction can be described as

$$BrO_3^- + 3H_2 \xrightarrow{Pd} Br^- + 3H_2O \quad (1)$$

For all three materials, BrO_3^- consumption was accompanied by Br^- production, and the sum of BrO_3^- and Br^- concentrations remained very close to the initial BrO_3^- concentration (see Figure S5 in the SI), confirming that the observed BrO_3^- loss from solution resulted from reduction of the oxyanion rather than adsorption to the high surface area material. None of the oxyanion intermediates (BrO_2^- and BrO^-) were detected, indicating that the reduction of such intermediates is much faster than that of BrO_3^-.

Comparing the time courses for BrO_3^- reduction observed with the three materials under neutral pH conditions (Figure 5A) reveals that the reaction with SiO_2@Pd@$mSiO_2$ proceeded much faster than with Pd NPs and SiO_2@Pd. Kinetics followed a pseudo-first-order rate law (Figure 5A), and the resulting rate constants (Pd mass normalized) were determined for all the experiments (see Table 1). Pseudo-first-order rate constants are typically used to describe the kinetics of different catalytic reduction experiments.[5,8,48−51] Similar rate constants for BrO_3^- reduction with Pd NPs and SiO_2@Pd were measured at pH 7 (Figure 5B). Thus, immobilization of Pd NPs onto silica supports did not decrease the apparent catalytic activity. Under these same pH conditions, which is highly relevant to water treatment applications, the rate constant for SiO_2@Pd@$mSiO_2$ was more than an order-of-magnitude larger than those obtained for Pd NPs and SiO_2@Pd (Figure 5B). Initial turnover frequency (TOF_0) values were also determined (Table 1); they followed the same trend as the pseudo-first-order rate constants. To the best of our knowledge, this is the first report of mesoporous-shell-enhanced activity of metal NPs in catalysis applications at ambient temperature. These results indicate that, in addition to the active metal sites, the structure of the solid supports play an important role in determining the

dx.doi.org/10.1021/cs500971r | ACS Catal. 2014, 4, 3551−3559

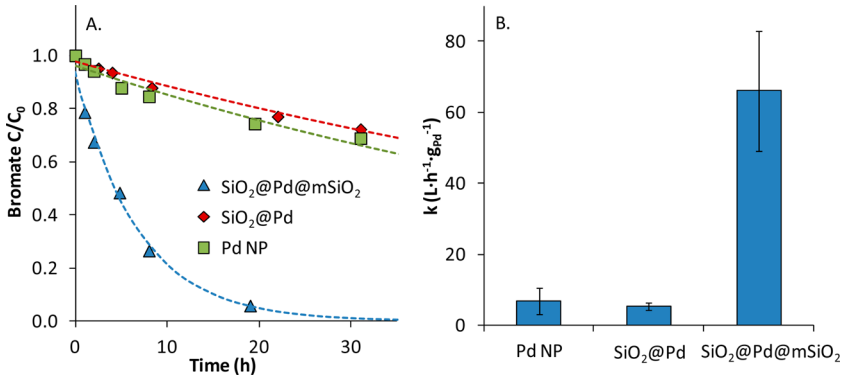

Figure 5. Reduction of 100 μM BrO_3^- by 2 mg_{Pd} L^{-1} loading of Pd NPs, SiO_2@Pd, and SiO_2@Pd@mSiO_2 in water at pH 7 (20 ± 1 °C, P_{H_2} = 1 atm): (A) Time courses for BrO_3^- reduction (dashed lines represent pseudo-first-order kinetics model fits); (B) Pd mass-normalized rate constants for BrO_3^- reduction (error bars represent one standard deviation determined from triplicate experiments).

Table 1. Results of Kinetics Experiments Measuring Catalytic Reduction of Bromate[a]

catalyst	pH	rate constant, k[b] (L h^{-1} g_{Pd}^{-1})	initial turnover frequency, TOF_0[b] (h^{-1})
Pd NP	7	6.88 (±3.69) × 10^0	0.30 (±0.16) × 10^0
SiO_2@Pd	8	2.47 (±0.53) × 10^0	0.21 (±0.05) × 10^0
SiO_2@Pd	7	5.45 (±1.03) × 10^0	0.47 (±0.09) × 10^0
SiO_2@Pd	6	1.56 (±0.55) × 10^1	1.34 (±0.47) × 10^0
SiO_2@Pd	4	5.07 (±0.66) × 10^2	4.35 (±0.57) × 10^1
SiO_2@Pd	2	2.62 (±0.65) × 10^3	2.25 (±0.56) × 10^2
SiO_2@Pd@mSiO_2	8	2.89 (±0.56) × 10^1	3.23 (±0.63) × 10^0
SiO_2@Pd@mSiO_2	7	6.60 (±1.69) × 10^1	7.40 (±1.89) × 10^0
SiO_2@Pd@mSiO_2	6	9.39 (±2.55) × 10^1	1.52 (±0.41) × 10^1
SiO_2@Pd@mSiO_2	4	4.96 (±0.29) × 10^2	5.56 (±0.33) × 10^1
SiO_2@Pd@mSiO_2	2	2.86 (±0.37) × 10^3	3.20 (±0.41) × 10^2

[a]All experiments were conducted at $[BrO_3^-]_0$ = 100 μM, T = 20 ± 1 °C, P_{H_2} = 1 atm, and catalyst loading equivalent to yield 2 mg_{Pd} L^{-1}. [b]Uncertainty represents one standard deviation derived from at least duplicate experiments.

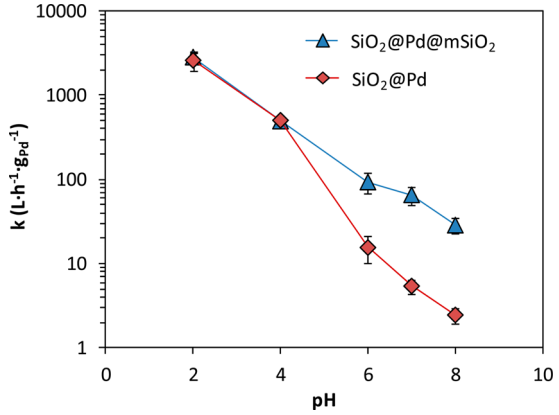

Figure 6. Influence of pH on rate constants for reduction of 100 μM BrO_3^- by 2 mg_{Pd} L^{-1} loading of SiO_2@Pd and SiO_2@Pd@mSiO_2 in water (T = 20 ± 1 °C, P_{H_2} = 1 atm). Error bars represent one standard deviation of replicate experiments.

activity of heterogeneous catalysts. The mechanism of enhancement is examined in a subsection below.

The effect of pH on reaction kinetics was determined for the two silica-supported catalysts (SiO_2@Pd and SiO_2@Pd@mSiO_2). BrO_3^- reduction rates increased with decreasing pH for both SiO_2@Pd and SiO_2@Pd@mSiO_2 (Figure 6). SiO_2@Pd@mSiO_2 was found to be much more active than SiO_2@Pd for pH 6–8, but activities for the two materials converged under more acidic conditions. Compared to metal- or metal-oxide-based supports, including alumina and iron, silica is not only stable under mild basic conditions (pH <12), but also is well-known for its high stability under acidic conditions.[52] Therefore, silica may potentially serve as an ideal candidate for a Pd NP support for catalytic applications in a wide pH range, including acidic media.

Solution pH may affect both the interaction between active Pd(0) sites and bromate, and the surface properties of the silica supports. Strong pH-dependent activities have been reported for catalytic reduction of oxyanions including bromate, nitrate, and perchlorate.[49,51,53] Hurley and Shapley investigated catalytic ClO_4^- reduction by a Pd/Re-based bimetallic catalyst.[49] They proposed that acidic condition promoted hydrogen bonding between ClO_4^- and the immobilized Re metal species, thereby accelerating oxygen atom transfer in the proposed reaction mechanism. Chen et al. found that the reduction rate of bromate increased with decreasing pH with an alumina supported Pd catalyst, and they attributed the pH-dependent activity to both the redox potential of bromate reduction and the surface properties of the catalyst.[53] The zeta potentials of SiO_2@Pd and SiO_2@Pd@mSiO_2 were measured in H_2-saturated aqueous solutions as a function of pH in this work (Figure 7). The surfaces of both SiO_2@Pd and SiO_2@Pd@mSiO_2 were less negatively charged with decreasing pH. Similar to others, we propose that less negative surface charge at lower pH increases electrostatic attractive interactions between BrO_3^- and the catalyst surfaces and increases the apparent reaction rate. It is worth noting that the presence of dissolved H_2 markedly affects the zeta potential of Pd-based catalyst surfaces, and here the addition of H_2(g) shifted the zeta potential of both SiO_2@Pd and SiO_2@Pd@mSiO_2 to a more negative values at a given pH (see Figure S6 in the SI). Similarly, Choe et al. reported negative shifts in the surface charge of Pd/C catalysts in the presence of H_2.[54] The negative shift of zeta potential may be attributed to the formation of activated H species, which may adsorb on the surface of Pd or react with support surface functional groups, leading to the formation of negatively charged species.[54]

dx.doi.org/10.1021/cs500971r | ACS Catal. 2014, 4, 3551–3559

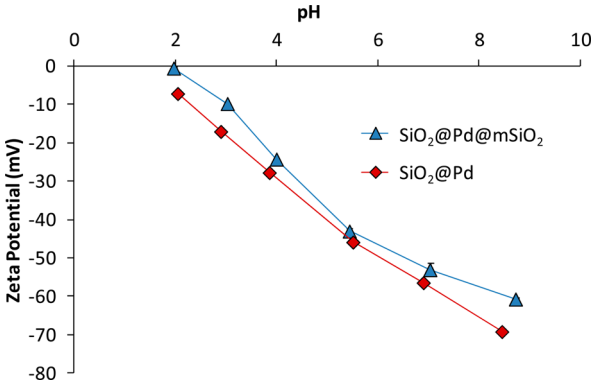

Figure 7. Influence of pH on the zeta potential of H_2-saturated aqueous suspensions of SiO_2@Pd and SiO_2@Pd@mSiO_2 (20 ± 1 °C, 1 atm H_2, 2 mg_{Pd} L^{-1} catalyst loading).

2.3. Discussion of Activity Enhancement of SiO_2@Pd@mSiO_2.

Potential reasons for enhanced catalytic activity of SiO_2@Pd@mSiO_2, relative to SiO_2@Pd, may be due to differences in the amount of active surface Pd(0) sites and the interaction between BrO_3^- and the catalyst surface. The amount of active surface Pd(0) sites is influenced by the total mass of Pd, the size and shape of the Pd NPs, and the accessibility of Pd NPs within the support matrix and can be evaluated by CO(g) chemisorption. For both SiO_2@Pd and SiO_2@Pd@mSiO_2, similar amounts of Pd octahedra with an average size of 6.2 nm were immobilized without evidence of NP aggregate formation. CO(g) chemisorption measurements yielded active Pd surface areas of 55 and 43 m^2/g of Pd for SiO_2@Pd and SiO_2@Pd@mSiO_2, respectively. This suggests that encapsulation in the mesoporous silica shell slightly reduces the Pd surface area available for reaction with BrO_3^-. Thus, enhanced reactive surface area cannot be the reason for the greater reactivity of SiO_2@Pd@mSiO_2.

A Langmuir–Hinshelwood (L-H) kinetic model was applied to provide insights into the interaction between BrO_3^- and the surface of catalysts. The L-H model has widely been applied to describe heterogeneous catalytic reaction kinetics.[3,50,55,56] According to the L-H model, catalytic hydrogenation reactions using Pd-based materials can be described by a series of steps,[3,50,55] involving rapid equilibrium adsorption of the target reactant and H_2 onto the surface of the catalyst, H_2 dissociation by Pd(0) to form reactive atomic hydrogen (H_{ads}), and reaction of H_{ads} with the target reactant. It is anticipated that (i) catalytic reduction of bromate by SiO_2@Pd@mSiO_2 and SiO_2@Pd follows these general steps, and (ii) diffusion limitations are negligible. The latter assumption is valid for the small particle sizes and rapid stirring rates used in this work.[56] The aqueous H_2 concentration was estimated as a constant of ~0.8 mM throughout the experiments, based on Henry's law for P_{H_2} = 1 atm, since H_2(g) was continuously sparged to the reactor.[52] Assuming that bromate and H_2 adsorb to the catalyst noncompetitively and that surface reaction is the rate-limiting step,[55,56] the corresponding L-H kinetic expression can be described as

$$R = k_{rxn}\left(\frac{K_{ads}[BrO_3^-]}{1 + K_{ads}[BrO_3^-]}\right) \quad (2)$$

where R is the rate of bromate reduction (mmol g_{Pd}^{-1} h^{-1}), k_{rxn} is the rate constant (mmol g_{Pd}^{-1} h^{-1}) for adsorbed BrO_3^- reacting with H_{ads} and is affected by the amount of the active surface Pd(0) sites, K_{ads} is the equilibrium adsorption constant (L $mmol^{-1}$) for bromate on the catalyst surface, and [BrO_3^-] is the aqueous bromate concentration (mmol L^{-1}).

Equation 2 was fit to the initial rates of BrO_3^- reduction by SiO_2@Pd and SiO_2@Pd@mSiO_2 measured for varying initial BrO_3^- concentration (see Figure 8), and parameters derived

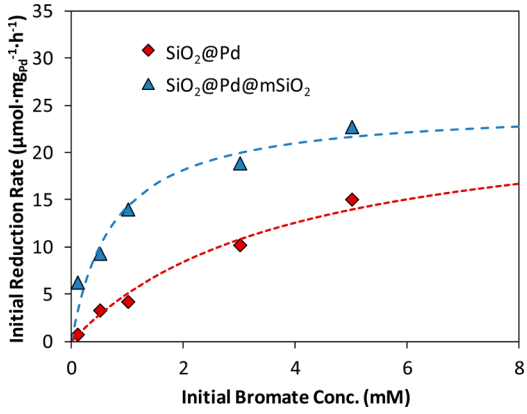

Figure 8. Influence of bromate concentration on the initial rate of aqueous bromate reduction by 2 mg_{Pd} L^{-1} loading of SiO_2@Pd and SiO_2@Pd@mSiO_2 (pH 7, 20 ± 1 °C, P_{H_2} = 1 atm). Dashed lines represent fits to the Langmuir–Hinshelwood (L-H) kinetics model.

from model fitting indicate that the presence of the mesoporous shell increases reactivity with BrO_3^- by enhancing oxyanion adsorption prior to reaction with H_{ads}. Based on chemisorption measurements, the amount of the active surface Pd(0) sites for SiO_2@Pd and SiO_2@Pd@mSiO_2 are similar, so a single k_{rxn} was assumed for the two materials during fitting. Simultaneous fitting (method of least-squares errors) of experimental data for both materials yielded an optimum value of k_{rxn} of 24.9 ± 4.7 mmol g_{Pd}^{-1} h^{-1} for both materials (uncertainty represents 95% confidence limits), but large differences in K_{ads}. The adsorption constant obtained for SiO_2@Pd@mSiO_2 (1.35 ± 0.87 L $mmol^{-1}$) was more than 5-fold larger than that obtained for SiO_2@Pd (0.26 ± 0.13 L $mmol^{-1}$). Although k_{rxn} was assumed to be the same for fits shown, fits conducted with independent k_{rxn} values also yielded good fits with similar k_{rxn} values and large differences in K_{ads} for the two materials. Thus, fitting indicates that the addition of the mesoporous shell serves to enhance the extent of BrO_3^- adsorption prior to reaction with H_{ads}. The model result is consistent with the experimental observation that the difference in activity between SiO_2@Pd and SiO_2@Pd@mSiO_2 decreased with increasing bromate concentration (see Figure 8) as sites near the Pd(0) source of H_{ads} become saturated with both materials. It should be mentioned that, while the adsorption constant increased by 5-fold for SiO_2@Pd@mSiO_2, little BrO_3^- adsorption was observed in H_2(g)-free control experiments for both SiO_2@Pd and SiO_2@Pd@mSiO_2, which is consistent with predictions from L-H K_{ads} values that <1% BrO_3^- adsorbs to both materials. Although the extent of adsorption is low for both materials (within the uncertainty level of the ion chromatography measurements for aqueous BrO_3^-), the 5-fold difference is critical to the net reaction kinetics because reaction occurs between adsorbed BrO_3^- and H species according to the L-H model. Therefore, results support a mechanism whereby oxyanion uptake by the high surface area

dx.doi.org/10.1021/cs500971r | ACS Catal. 2014, 4, 3551–3559

mesoporous shell enhances the overall rate of reduction in water.

We speculate that the increased K_{ads} for SiO_2@Pd@mSiO_2 results from the increase in silica surface sites for bromate adsorption near the source of reactive H_{ads}. While the specific surface area of the silica core is estimated as only ~1.4 m^2/g (based on spherical shape), the presence of the mesoporous shell significantly enhances the specific surface area of SiO_2@Pd@mSiO_2 to be 480 m^2/g (measured by BET). Theoretically, only bromate adsorbed on the active Pd(0) sites would be reduced to bromide since H_2 adsorption and activation would only occur on the active Pd(0) sites. However, bromate adsorbed to silica surface sites close to active Pd(0) sites may also be reactive, because of the possible spillover of H_{ads}. Hydrogen spillover is described as the dissociative chemisorption of H_2 onto an active metal site, followed by migration of the H_{ads} onto the surface of the support.[57,58] Previous studies suggest that H_{ads} typically only migrates a limited distance (in the nanometer range) from active metal sites of generation, because of the high energy for migration.[56] Hydrogen spillover has been widely observed in hydrogenation reactions in which carbon and silica are used as support materials.[57−59] A recent study has proposed that hydrogen spillover may enhance the activity of perchlorate reduction on Pd−Re/C.[51] It is possible that hydrogen spillover may also occur on silica supported Pd catalysts and reactions between the spilled H_{ads} and bromate adsorbed on the mesoporous shell results in an enhancement of the catalytic activity of SiO_2@Pd@mSiO_2.

An alternative rationale for the higher reactivity of SiO_2@Pd@mSiO_2 that was ruled out was a shift in the prevailing surface charge of the catalyst to favor uptake of the anionic BrO_3^- species. Zeta potential measurements conducted in H_2-saturated suspensions exhibited similar values for both SiO_2@Pd and SiO_2@Pd@mSiO_2 at all the pH values (Figure 7). Although the surface SiO_2@Pd was slightly more negative than SiO_2@Pd@mSiO_2, such a small difference cannot explain the 10-fold higher activity observed for SiO_2@Pd@mSiO_2 under neutral pH conditions.

3. CONCLUSIONS AND IMPLICATIONS

In the present work, Pd octahedral NPs with an average size of 6.2 nm were synthesized and immobilized in core−shell-structured silica materials (SiO_2@Pd and SiO_2@Pd@mSiO_2). A novel structured SiO_2@Pd@mSiO_2 was synthesized using a combination of techniques including sol−gel processing, interfacial deposition, and surfactant templating. Highly ordered mesopores with a uniform pore size of 2.3 nm were obtained for SiO_2@Pd@mSiO_2. Encapsulation between the nonporous core and mesoporous shell physically prevents detachment of the Pd NPs into the aqueous phase being treated and the open pore structure allows the reactants to reach the active surface Pd(0) sites. SiO_2@Pd@mSiO_2 showed much higher catalytic activity than unsupported Pd NPs and SiO_2@Pd for bromate reduction in water at neutral pH and ambient temperature. An L-H model was developed to describe the kinetics of catalytic BrO_3^- reduction and the elevated activity of SiO_2@Pd@mSiO_2, compared to SiO_2@Pd, was attributed to enhanced adsorption of BrO_3^- to the mesoporous shell prior to reaction of the oxyanion with H_{ads}.

Using bromate as a probe reactant, we demonstrate, for the first time, that encapsulation of shaped Pd NPs in mesoporous silica materials can significantly enhance the activity of catalyzed aqueous reactions at circumneutral pH, a condition that is most relevant to water purification applications. In addition to activity enhancement, the presence of the mesoporous shell may have additional benefits to environmental applications, including preventing NP aggregation and release, protecting the active metals from colloidal foulants, and potentially providing for the selective uptake of target solutes in complex aquatic matrices (e.g., by size exclusion or pore channel functionalization). The high stability of silica materials at low pH also makes them suitable for treating acidic water and wastewater. These results suggest that core−shell-structured mesoporous silica may serve as an ideal support for a wide range of metal nanomaterials that can potentially be used in different applications relevant to environmental treatment processes. Future work will be dedicated to (1) optimize the catalyst composition (e.g., Pd NP loading, size, and shape) to further enhance the activity; (2) determine the performance of the catalysts as well as Pd leaching and release in the presence of a number of water constituents; (3) assess the capability of the catalyst to remove a variety of emerging contaminants; (4) extend the methods demonstrated here to immobilize other metal or metal oxide nanomaterials with various shapes and sizes; and (5) evaluate the reusability and longevity of the catalysts in treatment applications in the field.

4. EXPERIMENTAL SECTION

4.1. Material Synthesis. Details of all the chemicals used in the present work, and methods of synthesis of Pd NPs, synthesis and surface modification of silica microspheres, and synthesis of SiO_2@Pd and SiO_2@Pd@mSiO_2, have been provided in the SI.

4.2. Catalytic Reduction of Bromate. The kinetics of bromate reduction by H_2 were measured in continuously stirred batch reactors at ambient temperature (20 ± 1 °C). Pd NPs, SiO_2@Pd, or SiO_2@Pd@mSiO_2 was added to a 50-mL round-bottom flask with a solid loading sufficient to yield a concentration of 2 $mg_{Pd}\ L^{-1}$. An aliquot of a phosphate stock solution was added to provide a phosphate concentration of 1 mM to buffer pH, and HCl or NaOH was used to adjust the solution pH to the desired value (pH 2−8). The reactor was then capped with a rubber stopper that contained two 16-gauge stainless steel needles, with one serving as the H_2 gas inlet and the other as both the gas outlet and the liquid sampling port. After sparging the catalyst suspension with H_2 for 30 min, the reaction was initiated by injecting bromate to yield the desired initial concentration (0.1−5 mM). Suspension aliquots were then collected periodically, immediately filtered (0.45 μm polytetrafluoroethylene (PTFE)) to quench reactions, and analyzed for BrO_3^- and Br^- concentrations. Each experimental condition was run at least in duplicate, except for those with initial bromate concentrations higher than 0.1 mM.

4.3. Analytical Methods. *Catalyst Characterization.* The shape and morphology of the synthesized Pd NPs, SiO_2@Pd, and SiO_2@Pd@mSiO_2 were determined by TEM and SEM. TEM images were acquired by a JEOL Model 2010LAB6 microscope operated at 200 kV. SEM images were taken using a Hitachi Model S4700 high-resolution microscope. N_2(g) adsorption−desorption isotherms were performed with a Micromeritics ASAP 2020 surface analyzer to measure the surface area and pore size distribution of SiO_2@Pd@mSiO_2. Specific surface area was calculated using the BET method, the pore volume and pore size distribution was obtained via BJH model, and the total pore volumes were obtained from the adsorbed quantity at a relative pressure (P/P_0) of 0.995. The

dx.doi.org/10.1021/cs500971r | ACS Catal. 2014, 4, 3551−3559

metallic Pd surface area of SiO_2@Pd and SiO_2@Pd@mSiO_2 was quantified using CO(g) chemisorption (Micromeritics ASAP 2020C). The samples were heated in H_2(g) at 350 °C for 2 h before performing CO chemisorption analysis at 35 °C. The crystalline phases of Pd NPs and SiO_2@Pd were determined by powder XRD measurement performed on a Bruker General Area Detector Diffraction System using Cu Kα radiation. The surface zeta potentials of SiO_2@Pd and SiO_2@Pd@mSiO_2 were measured with a Malvern Zetasizer ZS 90. To measure zeta potential, solids were added to a reactor with a loading of 2 mg_{Pd} L^{-1}. Phosphate (1 mM) was added as a pH buffer and pH was then adjusted to the desired value to mimic conditions used in bromate reduction kinetics experiments. After sparging with H_2 for 30 min, an aliquot of suspension was collected and measured immediately. Concentrations of Pd in Pd NP suspension, SiO_2@Pd, and SiO_2@Pd@mSiO_2 were quantified by inductively coupled plasma–optical emission spectrometry (ICP-OES) (Perkin–Elmer, Model Optima 2000 DV) after microwave digestion (Perkin–Elmer/AntonPaar Multiwave 3000) with HNO_3–H_2O_2.

Aqueous Analysis. Concentrations of bromate and bromide were quantified by ion chromatography with conductivity detection (IC-CD) (Dionex ICS-2000). An IonPac AS19 column maintained at 30 °C was used as the stationary phase, and a 32 mM KOH solution with a flow rate of 1.0 mL/min was used as the eluent. Solution pH was measured with a glass pH electrode and pH meter (Thermo Scientific).

■ ASSOCIATED CONTENT

Supporting Information

Details of chemicals; synthesis of Pd NPs; synthesis and surface modification of silica microspheres; synthesis of SiO_2@Pd and SiO_2@Pd@mSiO_2; determination of TOF_0; additional TEM and SEM images of as-synthesized materials; time courses of bromate reduction; zeta potential measurements with and without H_2. This material is available free of charge via the Internet at http://pubs.acs.org.

■ AUTHOR INFORMATION

Corresponding Author

*Tel.: 217-244-4679. E-mail: strthmnn@illinois.edu.

Present Addresses

[‖]Y. Wang: Department of Civil and Environmental Engineering University of Wisconsin-Milwaukee, Milwaukee, WI 53211 wang292@uwm.edu

[⊥]C. Werth: Dept. of Civil, Architectural and Environmental Engineering University of Texas at Austin, Austin, TX 78712 werth@utexas.edu

Author Contributions

[‡]These authors (Y.W. and J.L.) contributed to this work equally.

Notes

The authors declare no competing financial interest.

■ ACKNOWLEDGMENTS

This work was financially supported by the Academic Excellence Alliance (AEA) program at King Abdullah University of Science and Technology (KAUST) and NSF Chemical, Bioengineering, Environmental, and Transport Systems (No. CBET-0746453). We thank Jeffery Bertke and Rudiger Laufhutte (Department of Chemistry at the University of Illinois at Urbana–Champaign (UIUC)) for helping to acquire the XRD patterns and elemental analysis, respectively. We appreciate the help from Ruiqing Lu (UIUC) with obtaining the zeta potential measurements, and Dr. Shaoying Qi (UIUC) for gas adsorption experiments. Technical Assistance at KAUST was provided by Dr. Hongnan Zhang, Dr. Zhonghai Zhang, Mr. Rubal Dua and Mr. Guoying Chen. Four anonymous reviewers provided insightful comments to help improve the presentation of the results in this paper.

■ REFERENCES

(1) Beletskaya, I. P.; Cherpakov, A. V. *Chem. Rev.* **2000**, *100*, 3009–3066.

(2) Johansson Seechurn, C. C. C.; Kitching, M. O.; Colacot, T. J.; Snieckus, V. *Angew. Chem., Int. Ed.* **2012**, *51*, 5062–5085.

(3) Chaplin, B. P.; Reinhard, M.; Schneider, W. F.; Schüth, C.; Shapley, J. R.; Strathmann, T. J.; Werth, C. J. *Environ. Sci. Technol.* **2012**, *46*, 3655–3670.

(4) Chaplin, B. P.; Roundy, E.; Guy, K. A.; Shapley, J. R.; Werth, C. J. *Environ. Sci. Technol.* **2006**, *40*, 3075–3081.

(5) Chaplin, B. P.; Shapley, J. R.; Werth, C. J. *Environ. Sci. Technol.* **2007**, *41*, 5491–5497.

(6) Chinthaginjala, J. K.; Lefferts, L. *Appl. Catal., B* **2010**, *101*, 144–149.

(7) Davie, M. G.; Cheng, H. F.; Hopkins, G. D.; Lebron, C. A.; Reinhard, M. *Environ. Sci. Technol.* **2008**, *42*, 8908–8915.

(8) Shuai, D.; Chaplin, B. P.; Shapley, J. R.; Menendez, N. P.; McCalman, D. C.; Schneider, W. F.; Werth, C. J. *Environ. Sci. Technol.* **2010**, *44*, 1773–1779.

(9) Xiong, Y.; Xia, Y. *Adv. Mater.* **2007**, *19*, 3385–3391.

(10) Crespo-Quesada, M.; Yarulin, A.; Jin, M.; Xia, Y.; Kiwi-Minsker, L. *J. Am. Chem. Soc.* **2011**, *133*, 12787–12794.

(11) Xiong, Y.; Cai, H.; Wiley, B. J.; Wang, J.; Kim, M. J.; Xia, Y. *J. Am. Chem. Soc.* **2007**, *129*, 3665–3675.

(12) Xiong, Y.; Chen, J.; Wiley, B.; Xia, Y.; Aloni, S.; Yin, Y. *J. Am. Chem. Soc.* **2005**, *127*, 7332–7333.

(13) Shao, M.; Yu, T.; Odell, J. H.; Jin, M.; Xia, Y. *Chem. Commun.* **2011**, *47*, 6566–6568.

(14) Johnson, J. A.; Makis, J. J.; Marvin, K. A.; Rodenbusch, S. E.; Stevenson, K. J. *J. Phys. Chem. C* **2013**, *117*, 22644–22651.

(15) Zhao, Z.; Arentz, J.; Pretzer, L. A.; Limpornpipat, P.; Clomburg, J. M.; Gonzalez, R.; Schweitzer, N. M.; Wu, T.; Miller, J. T.; Wong, M. S. *Chem. Sci.* **2014**, *5*, 3715–3728.

(16) Fang, Y. L.; Heck, K. N.; Alvarez, P. J. J.; Wong, M. S. *ACS Catal.* **2011**, *1*, 128–138.

(17) Pretzer, L. A.; Song, H. J.; Fang, Y. L.; Zhao, Z.; Guo, N.; Wu, T.; Arslan, I.; Miller, J. T.; Wong, M. S. *J. Catal.* **2013**, *298*, 206–217.

(18) Shuai, D.; McCalman, D. C.; Choe, J. K.; Shapley, J. R.; Schneider, W. F.; Werth, C. J. *ACS Catal.* **2013**, *3*, 453–463.

(19) Diallo, A. K.; Ornelas, C.; Salmon, L.; Ruiz Aranzaes, J.; Astruc, D. *Angew. Chem., Int. Ed.* **2007**, *46*, 8644–8648.

(20) Thathagar, M. B.; ten Elshof, J. E.; Rothenberg, G. *Angew. Chem., Int. Ed.* **2006**, *45*, 2886–2890.

(21) Mazumder, V.; Sun, S. *J. Am. Chem. Soc.* **2009**, *131*, 4588–4589.

(22) Wilkinson, K. E.; Palmberg, L.; Witasp, E.; Kupczyk, M.; Feliu, N.; Gerde, P.; Seisenbaeva, G. A.; Fadeel, B.; Dahlén, S. E.; Kessler, V. G. *ACS Nano* **2011**, *5*, 5312–5324.

(23) Joo, S. H.; Park, J. Y.; Tsung, C. K.; Yamada, Y.; Yang, P.; Somorjai, G. A. *Nat. Mater.* **2009**, *8*, 126–131.

(24) Lee, J.; Park, J. C.; Song, H. *Adv. Mater.* **2008**, *20*, 1523–1528.

(25) Henning, A. M.; Watt, J.; Miedziak, P. J.; Cheong, S.; Santonastaso, M.; Song, M.; Takeda, Y.; Kirkland, A. I.; Taylor, S. H.; Tilley, R. D. *Angew. Chem., Int. Ed.* **2013**, *52*, 1477–1480.

(26) Polshettiwar, V.; Len, C.; Fihri, A. *Coord. Chem. Rev.* **2009**, *253*, 2599–2626.

(27) Li, W.; Zhao, D. *Adv. Mater.* **2013**, *25*, 142–149.

(28) Ge, J.; Zhang, Q.; Zhang, T.; Yin, Y. *Angew. Chem.* **2008**, *120*, 9056–9060.

(29) Westcott, S. L.; Oldenburg, S. J.; Lee, T. R.; Halas, N. J. *Langmuir* **1998**, *14*, 5396−5401.
(30) Yadav, M.; Singh, A. K.; Tsumori, N.; Xu, Q. *J. Mater. Chem.* **2012**, *22*, 19146−19150.
(31) Zeng, H. C. *Acc. Chem. Res.* **2012**, *46*, 226−235.
(32) Park, J. N.; Forman, A. J.; Tang, W.; Cheng, J.; Hu, Y. S.; Lin, H.; McFarland, E. W. *Small* **2008**, *4*, 1694−1697.
(33) Deng, Y.; Cai, Y.; Sun, Z.; Liu, J.; Liu, C.; Wei, J.; Li, W.; Liu, C.; Wang, Y.; Zhao, D. *J. Am. Chem. Soc.* **2010**, *132*, 8466−8473.
(34) Wang, Y.; Biradar, A. V.; Duncan, C. T.; Asefa, T. *J. Mater. Chem.* **2010**, *20*, 7834−7841.
(35) Haag, W. R.; Hoigne, J. *Environ. Sci. Technol.* **1983**, *17*, 261−267.
(36) Weinberg, H. S.; Delcomyn, C. A.; Unnam, V. *Environ. Sci. Technol.* **2003**, *37*, 3104−3110.
(37) Kurokawa, Y.; Maekawa, A.; Takahashi, M.; Hayashi, Y. *Environ. Health Perspect.* **1990**, *87*, 309−335.
(38) Stöber, W.; Fink, A.; Bohn, E. *J. Colloid Interface Sci.* **1968**, *26*, 62−69.
(39) Kooij, E. S.; Brouwer, E. A. M.; Wormeester, H.; Poelsema, B. *Langmuir* **2002**, *18*, 7677−7682.
(40) Howarter, J. A.; Youngblood, J. P. *Langmuir* **2006**, *22*, 11142−11147.
(41) Westcott, S. L.; Oldenburg, S. J.; Lee, T. R.; Halas, N. J. *Chem. Phys. Lett.* **1999**, *300*, 651−655.
(42) Wang, Q.; Liu, H.; Wang, H. *J. Colloid Interface Sci.* **1997**, *190*, 380−386.
(43) Grabar, K. C.; Allison, K. J.; Baker, B. E.; Bright, R. M.; Brown, K. R.; Freeman, R. G.; Fox, A. P.; Keating, C. D.; Musick, M. D.; Natan, M. J. *Langmuir* **1996**, *12*, 2353−2361.
(44) Wan, Y.; Zhao, D. *Chem. Rev.* **2007**, *107*, 2821−2860.
(45) Inagaki, S.; Sakamoto, Y.; Fukushima, Y.; Terasaki, O. *Chem. Mater.* **1996**, *8*, 2089−2095.
(46) Yoon, S. B.; Kim, J. Y.; Kim, J. H.; Park, Y. J.; Yoon, K. R.; Park, S. K.; Yu, J. S. *J. Mater. Chem.* **2007**, *17*, 1758−1761.
(47) Tan, B.; Rankin, S. E. *J. Phys. Chem. B* **2004**, *108*, 20122−20129.
(48) Davie, M. G.; Reinhard, M.; Shapley, J. R. *Environ. Sci. Technol.* **2006**, *40*, 7329−7335.
(49) Hurley, K. D.; Shapley, J. R. *Environ. Sci. Technol.* **2007**, *41*, 2044−2049.
(50) Lowry, G. V.; Reinhard, M. *Environ. Sci. Technol.* **1999**, *33*, 1905−1910.
(51) Liu, J.; Choe, J. K.; Sasnow, Z.; Werth, C. J.; Strathmann, T. J. *Water Res.* **2013**, *47*, 91−101.
(52) Benjamin, M. M. *Water Chemistry*; McGraw−Hill: New York, 2002; pp 641−647.
(53) Chen, H.; Xu, Z.; Wan, H.; Zheng, J.; Yin, D.; Zheng, S. *Appl. Catal., B* **2010**, *96*, 307−313.
(54) Choe, J. K.; Shapley, J. R.; Strathmann, T. J.; Werth, C. J. *Environ. Sci. Technol.* **2010**, *44*, 4716−4721.
(55) Lowry, G. V.; Reinhard, M. *Environ. Sci. Technol.* **2001**, *35*, 696−702.
(56) Vannice, M. A. *Kinetics of Catalytic Reactions*; Springer: New York, 2005; pp 141−207.
(57) Prins, R. *Chem. Rev.* **2012**, *112*, 2714−2738.
(58) Conner, W. C.; Falconer, J. L. *Chem. Rev.* **1995**, *95*, 759−788.
(59) Beaumont, S. K.; Alayoglu, S.; Specht, C.; Kruse, N.; Somorjai, G. A. *Nano Lett.* **2014**, *14*, 4792−4796.